Advanced Physical Research
Vol.4, No.2, 2022, pp.69-80

Au_{53}: A STRONGEST SUPER TRIPLE-STATE DEGREES OF DEGENERACY IN METALLIC NANOCLUSTERS, $Au_{51-54}(C_1)$

K. Vishwanathan*

Faculty of Natural Sciences and Technology, University of Saarland, 66123, Saarbrücken, Germany

Abstract. In this article, an interesting phenomenon has described the geometries and vibrational frequency of the stable Au_N clusters with N = 51 to 54. We have found all 4 clusters are having the very same C_1 point symmetry group. For the re-optimization process, the finite-differentiation method has been implemented within the density-functional tight-binding (DFTB) approach. The effects of the range of interatomic forces were calculated and the desired set of system eigen frequencies (3N-6) are obtained by diagonalization of the symmetric positive semidefinite Hessian matrix. More than anything else, we have observed the vibrational spectra, which occur between 1.41 and 382.46 cm^{-1} at ΔE = 0. Most significantly, all the clusters had come across the double and triple-state degeneracies, which are due to the stretching and the bending mode of the vibrations through the atoms. Nevertheless, the vibrational spectrum is strongly dependent upon size, shape, and structure.

Keywords: *Gold Atomic Clusters, Density-Functional Tight-Binding (DFTB) approach, Finite-Difference Method, Force Constants (FCs) and Vibrational Spectrum.*

Corresponding Author: *K. Vishwanathan, Faculty of Natural Sciences and Technology, University of Saarland, 66123, Saarbrücken, Germany, e-mail: vishwak9@yahoo.com*

Received: *30 June 2022;* ***Accepted:*** *14 July 2022;* ***Published:*** *30 August 2022.*

1. Introduction

Nanoclusters have potential uses in chemical reactors, telecommunications, microelectronics, optical data storage, catalysts magnetic storage, spintronic devices, electroluminescent displays, sensors, biological markers, switches, nano-electronics, nano-optics, transducers and many other fields (Wu *et al*., 2016, Andres *et al*., 1996). In general, noble-metal (Cu, Ag, and Au) clusters have attracted much attention in scientific and technological fields because of their thermodynamic, electronic, optical and catalytic properties in nanomaterials (Choi *et al.*, 2007; Li *et al.*, 2016; Zhang *et al.*, 2019). Especially, gold is a soft metal and is usually alloyed to give it more strength as well as a good conductor of heat and electricity, and is unaffected by air and most reagents, those are the main reasons to choose among the other metal clusters.

Noble metal like rhodium (Rh), palladium (Pd), silver (Ag), platinum (Pt), and gold (Au) is one kind of modish and desired material, according to their inherent resistance to oxidation and corrosion even in the moist environment (Griffith, 1967; Hartley, 1973; Huang, 2016). Its physical and chemical properties appear to entirely change as the size of metal continuously decreases to the nanoscale because of the quantum size effect, surface effect, small size effect, and *macroscopic quantum tunnelling* (MQT) effect (Siegel, 1994; Huang *et al*., 2019).

In this study, mainly we focus on the vibrational properties of gold atomic clusters with sizes $Au_{51\text{-}54}$ atoms, because, the vibrational properties play a major role in the

structural stability (Garzon *et al*., 1996; Bravo-Perez *et al*., 1999; Bravo-Perez *et al*., 1999; Sauceda *et al*., 2012; Sauceda *et al*., 2013; Sauceda *et al*., 2015; Dugan & Erkoç, 2008). For further assistance for the readers, specifically for the general information about global minima gold structures which have been calculated by the work of Dong and Springborg (Dong & Springborg, 2007; Warnke, 2007) can be found in those articles. In very short, the structures were found through a so-called genetic algorithm (GA) in combination with Density Functional Tight-Binding (DFTB) energy calculations and the steepest descent algorithm permitting a local total energy minimization. Nevertheless, in our case, we use the numerical finite-difference method (Dvornikov, 2004) along with the density-functional tight-binding (DFTB) approach and finally extract the vibrational spectrum (of the numerical force constants) from the optimized structures. Overall, for a better understanding and visualization, detailed information is discussed in the results and discussion section.

2. Theoretical and Computational Procedures

At first step, the DFTB (Porezag *et al*., 1995; Seifert, 1992; Seifert *et al*., 1996) is based on the density functional theory of Hohenberg and Kohn in the formulation of Kohn and Sham. In addition, the Kohn-Sham orbitals $\psi_i(\mathbf{r})$ of the system of interest are expanded in terms of atom-centered basis functions $\{\varphi_m(\mathbf{r})\}$,

$$\psi i(\boldsymbol{r}) = \sum_m c_{im}\phi_m(\boldsymbol{r}),\ m = j. \tag{1}$$

While so far the variational parameters have been the real-space grid representations of the pseudo wave functions, it will now be the set of coefficients c_{im}. Index m describes the atom, where ϕ_m is centered and it is angular as well as radially dependent. The ϕ_m is determined by self-consistent DFT calculations on isolated atoms using large Slater-type basis sets.

In calculating the orbital energies, we need the Hamilton matrix elements and the overlap matrix elements. The above formula gives the secular equations

$$\sum_m c_{im}\,(H_{mn} - \epsilon_i S_{mn}) = 0 \tag{2}$$

Here, c_{im}'s are expansion coefficients, ϵ_i is for the single-particle energies (or where ϵ_i are the Kohn-Sham eigenvalues of the neutral), and the matrix elements of Hamiltonian H_{mn} and the overlap matrix elements S_{mn} are defined as

$$H_{mn} = \langle\phi_m|\widehat{H}|\phi_n\rangle, \qquad S_{mn} = \langle\phi_m|\phi_n\rangle \tag{3}$$

They depend on the atomic positions and on a well-guessed density $\rho(\mathbf{r})$. By solving the Kohn-Sham equations in an effective one particle potential, the Hamiltonian $\widehat{H}$ is defined as

$$\widehat{H}\psi_i(\mathrm{r}) = \epsilon_i\psi_i(\mathrm{r}), \widehat{H} = \widehat{T} + V_{eff}(\mathrm{r}) \tag{4}$$

To calculate the Hamiltonian matrix, the effective potential V_{eff} has to be approximated. Here, $\hat{T}$ being the kinetic-energy operator $\sum(\hat{T} = -\frac{1}{2}\nabla^2)$ and $V_{eff}(\mathbf{r})$ being the effective Kohn-Sham potential, which is approximated as a simple superposition of the potentials of the neutral atoms,

$$V_{eff}(\mathrm{r}) = \sum_j V_j^0\left(|r - R_j|\right) \quad (5)$$

V_j^0 is the Kohn-Sham potential of a neutral atom, $r_j = r - R_j$ is an atomic position, and R_j being the coordinates of the j -th atom.

Finally, the short-range interactions can be approximated by simple pair potentials, and the total energy of the compound of interest relative to that of the isolated atoms is then written as,

$$E_{tot} \simeq \sum_i \epsilon_i - \sum_j \sum_{m_j}^{occ} \epsilon_{jm_j} + \frac{1}{2}\sum_{j\neq j'} U_{jj'}\left(|\boldsymbol{R_j} - \boldsymbol{R_{j'}}|\right),$$
$$\epsilon_B \equiv \sum_i^{occ} \epsilon_i - S\sum_j \sum_{m_j}^{occ} \epsilon_{jm_j} \quad (6)$$

Here, the majority of the binding energy (ϵ_i) is contained in the difference between the single-particle energies ϵ_i of the system of interest and the single-particle energies ϵ_{jm_j} of the isolated atoms (atom index *j*, orbital index m_j), $U_{jj'}\left(|\boldsymbol{R_j} - \boldsymbol{R_{j'}}|\right)$ is determined as the difference between ϵ_B and ϵ_B^{SCF} for diatomic molecules (with E^{SCF} being the total energy from parameter-free density-functional calculations). In the present study, only the $5d$ and $6s$ electrons of the gold atoms are explicitly included, whereas the rest are treated within a frozen-core approximation (Porezag *et al*., 1995; Seifert *et al*., 1996; Seifert, 2007).

2.1. Structural re-optimization process

In our case, we have calculated the numerical first-order derivatives of the forces ($\mathbf{F}_{i\alpha}, \mathbf{F}_{i\beta}$) instead of the numerical-second-order derivatives of the total energy (E_{tot}). In principle, there is no difference, but numerically the approach of using the forces is more accurate (Dvornikov, 2004).

$$\frac{1}{M}\frac{\partial^2 E_{tot}}{\partial \boldsymbol{R}_{i\alpha}\partial \boldsymbol{R}_{j\beta}} = \frac{1}{M}\frac{1}{2ds}\left[\frac{\partial}{\partial \boldsymbol{R}_{i\alpha}}\left(-\boldsymbol{F}_{j\beta}\right) + \frac{\partial}{\partial \boldsymbol{R}_{j\beta}}\left(-\boldsymbol{F}_{i\alpha}\right)\right] \quad (7)$$

Here, F is a restoring forces which is acting upon the atoms, ds is a differentiation step-size and *M* represents the atomic mass, for homo-nuclear case. The complete list of these force constants (FCs) is called the Hessian *H*, which is a *(3N ×3N)* matrix. Here, i is the component of (x, y or z) of the force on the *j*-th atom, so we get $3N$ (Press *et al*., 2007).

3. Results and Discussion

The optimized structure of the clusters Au_{51-54}

We present the vibrational spectrum analysis of the re-optimized Au_{51-54} clusters, interestingly, all of them are having the very same point group symmetry C_1 at the ground state, ΔE = 0. Initially, the structures were found through a so-called genetic algorithm (GA) in combination with Density Functional Tight-Binding (DFTB) energy calculations and the steepest descent algorithm permitting a local total energy minimization (Dong & Springborg, 2007). To sum up, we have accurately predicted the vibrational frequency of the clusters, and they are very strongly dependent on the size, the structure, and the shape of the clusters, moreover, the effect is influenced by the stretching and the bending mode vibrations of the atoms those are due to changes on the

bond length fluctuations for a small step-size *ds* = ± 0.01 a.u. on the equilibrium coordinates (Vishwanathan, 2018). Nonetheless, for the perspective view of the structures, we have plotted with two different styles (Space-filling, Polyhedral).

3.1. The vibrational frequency (ω_i) range of the cluster Au_{51} at $\Delta E = 0$

Table 1 shows the low (at the least) and the high (at the most) frequency range of the cluster Au_{51}, which occurs between 3.67 and 299.21 cm^{-1}, and the lowest energy geometrical structural view can be seen in Fig 1.

Table 1. The Normal modes (NVM) and the vibrational frequencies (ω_i) of Au_{51} at $\Delta E = 0$

NVM (3N-6)	ω_i [cm^{-1}]	NVM (3N-6)	ω_i [cm^{-1}]	NVM (3N-6)	ω_i [cm^{-1}]	NVM (3N-6)	ω_i [cm^{-1}]
1	3.67	40	36.10	79	88.36	118	189.78
2	4.65	41	36.42	80	90.65	119	190.59
3	5.98	42	37.63	81	93.91	120	195.03
4	6.44	43	38.34	82	94.11	121	195.92
5	7.99	44	39.45	83	95.37	122	196.51
6	8.41	45	41.38	84	98.25	123	201.85
7	8.61	46	42.36	85	99.93	124	206.05
8	9.42	47	43.92	86	102.58	125	206.91
9	9.83	48	44.28	87	106.37	126	208.76
10	10.38	49	46.76	88	110.95	127	209.90
11	10.97	50	47.91	89	111.72	128	212.87
12	12.27	51	49.84	90	113.90	129	216.21
13	12.84	52	50.15	91	115.21	130	218.78
14	13.40	53	52.13	92	117.59	131	220.40
15	13.57	54	52.89	93	119.87	132	226.15
16	14.97	55	54.02	94	122.46	133	227.59
17	15.25	56	54.50	95	123.91	134	229.91
18	15.99	57	55.19	96	125.86	135	231.33
19	16.51	58	57.44	97	128.52	136	240.15
20	17.36	59	57.94	98	130.32	137	244.10
21	17.67	60	59.31	99	132.42	138	245.29
22	18.90	61	61.10	100	138.10	139	246.06
23	19.23	62	61.82	101	142.15	140	252.55
24	21.21	63	63.92	102	144.55	141	257.88
25	22.24	64	64.90	103	147.00	142	261.98
26	22.92	65	66.90	104	153.18	143	269.94
27	23.97	66	68.38	105	155.04	144	275.32
28	24.06	67	71.94	106	156.25	145	281.16
29	25.23	68	72.45	107	156.73	146	287.49
30	25.82	69	73.48	108	158.34	147	299.21
31	26.21	70	74.29	109	165.79	148	-
32	27.32	71	76.42	110	166.85	149	-
33	27.64	72	77.82	111	167.79	150	-
34	28.96	73	80.63	112	168.57	151	-
35	30.21	74	81.25	113	175.13	152	-
36	31.56	75	82.72	114	179.43	153	-
37	32.78	76	83.83	115	181.86	154	-
38	33.48	77	85.58	116	183.74	155	-
39	34.28	78	86.49	117	185.14	156	-

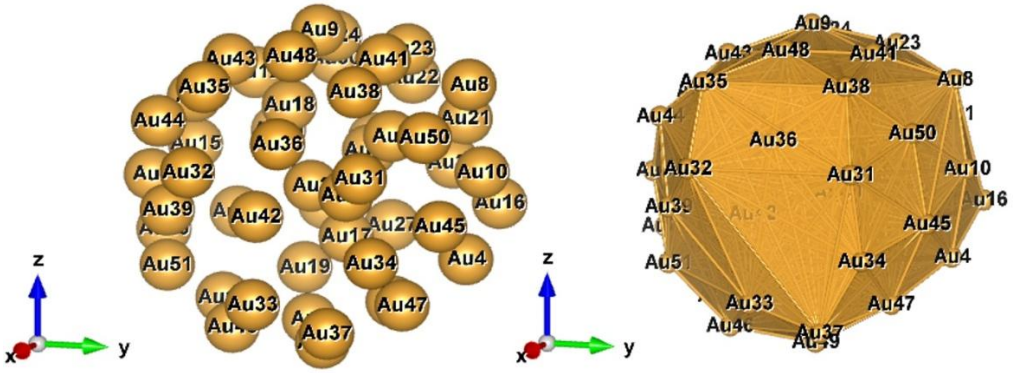

Fig. 1. Au_{51} (C_1); Style (Space-filling [left], Polyhedral [right]): The lowest energy geometrical structure of the Au_{51} cluster. Standard orientation of crystal shape at $\Delta E = 0$

Firstly, the cluster has some low frequencies (ω_{min}) between 3.67-9.83 cm^{-1}, which is only for the very first 9 NVM that comes even below the scale of Far Infrared FIR, IR-C 200-10 cm^{-1}.

Secondly, for the 10-122 NVM, the frequency ranges are occurred in between 10.38-196.51 cm^{-1}, which comes within the range of Far Infrared FIR, IR-C 200- 10 cm^{-1}.

Thirdly, the rest of the 123-147 NVM, are having the maximum high frequencies, which are ((ω_i) - 201.85-299.21 cm^{-1}) falling within the range of Mid Infrared MIR, IR-C 3330-200 cm^{-1}.

The double state degeneracy (ω_i): [{8.41, 8.61}; {9.42, 9.83}; {10.38, 10.97}; {12.27, 12.84}; {13.40, 13.57}; {15.25, 15.99}; {17.36, 17.67}; {22.24, 22.92}; {25.23, 25.82}; {27.32, 27.64}; {36.10, 36.42}; {52.13, 52.89}; {54.02, 54.50}; {57.44, 57.94}; {61.10, 61.82}; {156.25, 156.73}; {195.03, 195.92} and {206.05, 206.91}] in cm^{-1}.

The triple state degeneracy (ω_i): We do not find anything; it is clearly revealed through our spectrum calculations that have not occurred.

3.2. The vibrational frequency (ω_i) range of the cluster Au_{52} at $\Delta E = 0$

Table 2 shows the low (at the least) and the high (at the most) frequency range of the cluster Au_{52}, which occurs between 2.40 and 304.36 cm^{-1}, and the lowest energy geometrical structural view can be seen in Fig 2.

Firstly, the cluster has some low frequencies (ω_{min}) between 2.40-9.01 cm^{-1}, which is only for the very first 10 NVM that comes even below the scale of Far Infrared FIR, IR-C 200-10 cm^{-1}.

Secondly, for the 11-124 NVM, the frequency ranges occurred between 10.04-199.20 cm^{-1}, which comes within the range of Far Infrared FIR, IR-C 200- 10 cm^{-1}.

Thirdly, the rest of the 125-150 NVM, are having the maximum high frequencies, which are ((ω_i) - 201.97-304.36 cm^{-1}) falling within the range of Mid Infrared MIR, IR-C 3330-200 cm^{-1}.

The double and the triple state degeneracy (ω_i): [{5.21, 5.88}; {6.46, 6.77}; {10.04, 10.67}; {14.02, 14.31}; {15.54, 15.91}; {17.07, 17.62}; {22.09, 22.91}; {25.18, 25.40}; {32.50, 32.60}; {35.44, 35.50}; {37.28, 37.52, 37.74}; {43.39, 43.64}; {47.02, 47.76}; {51.49, 51.55}; {61.03, 61.32}; {78.12, 78.92}; {83.55, 83.82} and {198.19, 198.81}] in cm^{-1}.

3.3. The vibrational frequency (ω_i) range of the cluster Au_{53} at $\Delta E = 0$

Table 3 shows the low (at the least) and the high (at the most) frequency range of the cluster Au_{53}, which occurs between 1.41 and 382.46 cm^{-1}, and the lowest energy geometrical structural view can be seen in Fig 3.

Firstly, the cluster has some low frequencies (ω_{min}) between 1.41-9.55 cm^{-1}, which is only for the very first 12 NVM, which comes even below the scale of Far Infrared FIR, IR-C 200-10 cm^{-1}.

Secondly, for the 13-124 NVM, the frequency ranges occurred between 11.26-198.64 cm^{-1}, which comes within the range of Far Infrared FIR, IR-C 200- 10 cm^{-1}.

Thirdly, the rest of the 125-153 NVM, are having the maximum high frequencies, which are ((ω_i) - 200.46-382.46 cm^{-1}) falling within the range of Mid Infrared MIR, IR-C 3330-200 cm^{-1}.

Table 2. The Normal modes (NVM) and the vibrational frequencies (ω_i) of Au_{52} at $\Delta E = 0$

NVM (3N-6)	ω_i [cm^{-1}]	NVM (3N-6)	ω_i [cm^{-1}]	NVM (3N-6)	ω_i [cm^{-1}]	NVM (3N-6)	ω_i [cm^{-1}]
1	2.40	40	37.52	79	88.26	118	183.20
2	3.34	41	37.74	80	89.84	119	188.12
3	4.39	42	39.24	81	91.58	120	191.26
4	5.21	43	40.03	82	93.78	121	193.14
5	5.88	44	41.35	83	94.06	122	198.19
6	6.46	45	42.24	84	94.82	123	198.81
7	6.77	46	43.39	85	98.52	124	199.20
8	7.45	47	43.64	86	101.01	125	201.97
9	8.37	48	45.54	87	102.90	126	204.67
10	9.01	49	47.02	88	105.43	127	208.53
11	10.04	50	47.76	89	106.13	128	210.65
12	10.67	51	48.24	90	108.24	129	213.50
13	11.99	52	50.29	91	110.44	130	215.17
14	13.21	53	51.49	92	111.05	131	219.67
15	14.02	54	51.55	93	116.07	132	223.79
16	14.31	55	52.85	94	117.68	133	227.91
17	15.54	56	53.99	95	120.46	134	229.91
18	15.91	57	55.67	96	123.03	135	231.08
19	17.07	58	57.98	97	126.04	136	236.23
20	17.62	59	59.35	98	128.43	137	240.06
21	18.01	60	61.03	99	131.16	138	243.53
22	19.00	61	61.32	100	132.18	139	247.26
23	20.79	62	62.80	101	133.99	140	248.08
24	22.09	63	64.85	102	140.64	141	251.85
25	22.91	64	65.84	103	143.93	142	253.98
26	25.18	65	67.90	104	146.25	143	258.86
27	25.40	66	68.01	105	147.31	144	260.43
28	26.86	67	71.60	106	150.60	145	266.09
29	27.56	68	72.11	107	152.09	146	277.91
30	28.08	69	73.64	108	154.91	147	289.97
31	29.47	70	75.54	109	158.70	148	299.24
32	30.72	71	77.28	110	160.41	149	301.86
33	31.57	72	78.12	111	161.92	150	304.36
34	32.50	73	78.92	112	168.52	151	-
35	32.60	74	80.93	113	171.65	152	-
36	34.35	75	83.55	114	172.56	153	-
37	35.44	76	83.82	115	176.73	154	-
38	35.50	77	85.35	116	178.53	155	-
39	37.28	78	87.58	117	179.96	156	-

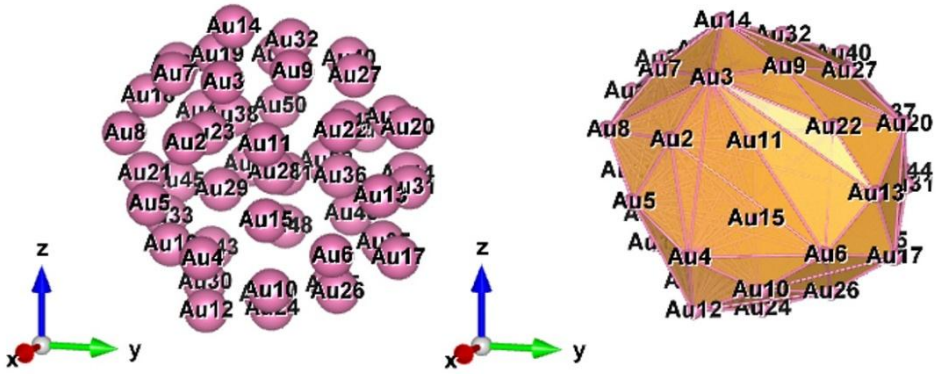

Fig. 2. Au_{52} (C_1); Style (Space-filling [left], Polyhedral [right]): The lowest energy geometrical structure of the Au_{52} cluster. Standard orientation of crystal shape at $\Delta E = 0$

Table 3. The Normal modes (NVM) and the vibrational frequencies (ω_i) of Au_{53} at $\Delta E = 0$

NVM (3N-6)	ω_i [cm^{-1}]	NVM (3N-6)	ω_i [cm^{-1}]	NVM (3N-6)	ω_i [cm^{-1}]	NVM (3N-6)	ω_i [cm^{-1}]
1	1.41	40	33.87	79	85.32	118	179.56
2	1.82	41	35.10	80	85.81	119	182.12
3	2.43	42	36.43	81	87.64	120	184.65
4	3.88	43	37.80	82	90.79	121	187.65
5	5.50	44	39.15	83	93.64	122	190.72
6	6.76	45	39.51	84	94.19	123	192.56
7	7.03	46	41.10	85	97.89	124	198.64
8	7.25	47	42.23	86	99.30	125	200.46
9	7.45	48	43.30	87	100.29	126	206.46
10	8.38	49	44.69	88	103.04	127	210.57
11	8.68	50	46.08	89	105.55	128	212.28
12	9.55	51	47.00	90	107.35	129	214.19
13	11.26	52	47.34	91	111.66	130	214.85
14	11.59	53	48.40	92	114.91	131	219.94
15	11.94	54	48.87	93	115.34	132	224.63
16	12.89	55	49.63	94	118.66	133	226.42
17	13.67	56	50.77	95	119.66	134	230.05
18	13.92	57	52.08	96	122.91	135	232.13
19	14.79	58	53.10	97	123.53	136	234.10
20	15.38	59	54.45	98	125.54	137	236.72
21	16.58	60	55.79	99	128.08	138	246.17
22	18.17	61	56.71	100	130.88	139	251.57
23	18.51	62	58.12	101	132.61	140	253.21
24	18.82	63	60.26	102	135.04	141	256.86
25	19.36	64	61.38	103	135.42	142	259.71
26	20.21	65	62.33	104	139.25	143	263.73
27	21.13	66	62.89	105	143.94	144	271.27
28	21.49	67	63.83	106	145.38	145	278.58
29	22.18	68	66.50	107	146.97	146	288.40
30	24.13	69	67.78	108	148.46	147	289.47
31	26.34	70	68.96	109	149.96	148	295.27
32	26.52	71	72.15	110	152.71	149	297.73
33	27.37	72	72.79	111	159.47	150	301.36
34	27.69	73	74.14	112	161.97	151	314.79
35	28.69	74	76.71	113	164.44	152	322.04
36	29.57	75	78.96	114	167.14	153	382.46
37	30.58	76	79.97	115	168.82	154	-
38	31.94	77	82.36	116	174.03	155	-
39	32.59	78	83.89	117	176.78	156	-

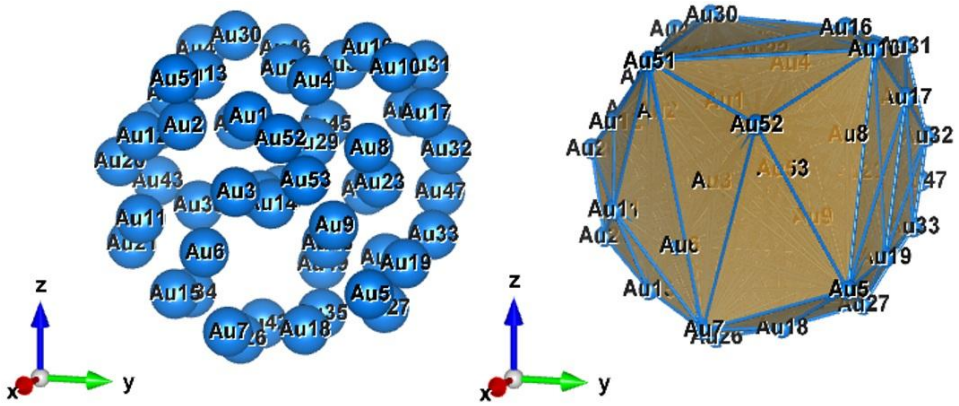

Fig. 3. Au_{53} (C_1); Style (Space-filling [left], Polyhedral [right]): The lowest energy geometrical structure of the Au_{53} cluster. Standard orientation of crystal shape at $\Delta E = 0$

The double and the triple state degeneracy (ω_i): [{1.41, 1.82}; {7.03, 7.25, 7.45}; {8.38, 8.68}; {11.26, 11.59, 11.94}; {13.67, 13.92}; {18.17, 18.51, 18.82}; {21.13, 21.49}; {26.34, 26.52}; {27.37, 27.69}; {39.15, 39.51}; {47.00, 47.34}; {48.40, 48.87}; {62.33, 62.89}; {72.15, 72.79}; {85.32, 85.81}; {135.04, 135.42} and {214.19, 214.85}] in cm^{-1}. More triple states (T^3) occurred than in the other clusters (refer to table A).

3.4. The vibrational frequency (ω_i) range of the cluster Au_{54} at $\Delta E = 0$

Table 4 shows the low (at the least) and the high (at the most) frequency range of the cluster Au_{54}, which occurs between 1.46 and 305.16 cm^{-1}, and the lowest energy geometrical structural view can be seen in Fig 4.

Firstly, the cluster has some low frequencies (ω_{min}) between 1.46-9.09 cm^{-1}, which is only for the very first 10 NVM, which comes even below the scale of Far Infrared FIR, IR-C 200-10 cm^{-1}.

Secondly, for the 11-130 NVM, the frequency ranges occurred between 10.08-198.54 cm^{-1}, which comes within the range of Far Infrared FIR, IR-C 200- 10 cm^{-1}.

Thirdly, the rest of the 131-156 NVM, are having the maximum high frequencies, which are ((ω_i) - 200.78-305.16 cm^{-1}) falling within the range of Mid Infrared MIR, IR-C 3330-200 cm^{-1}.

A spinning top on the Au_{54} cluster and the future usages: Our sky-line (outline) shape of the cluster resembles the very same as a spinning-top, as well as having the core-shell at the center, and it can be seen through the perspective structural view, and one of the atoms on the Au_{54} cluster is located at the corner or spin top. As a result, as a tip of the whole core-shell structure that can easily help to connect with any other possible molecules with ligand or catalyst, as a result, that will lead to producing new bio-electronics, nano electric devices, etc. Additionally, in one of our previous works, we found a very similar shape on the cluster Au_{25} (Vishwanathan, 2021).

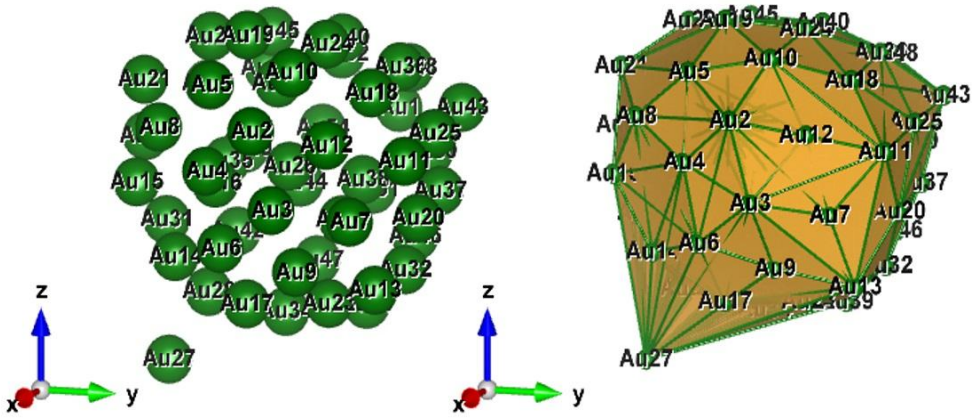

Fig. 4. Au_{54} (C_1); Style (Space-filling [left], Polyhedral [right]): The lowest energy geometrical structure of the Au_{54} cluster. Standard orientation of crystal shape at $\Delta E = 0$

Table 4. The Normal modes (NVM) and the vibrational frequencies (ω_i) of Au_{54} at $\Delta E = 0$.

NVM (3N-6)	ω_i [cm^{-1}]	NVM (3N-6)	ω_i [cm^{-1}]	NVM (3N-6)	ω_i [cm^{-1}]	NVM (3N-6)	ω_i [cm^{-1}]
1	1.46	40	34.07	79	81.03	118	168.07
2	4.22	41	34.46	80	82.27	119	171.19
3	4.65	42	34.77	81	83.89	120	172.91
4	5.07	43	35.47	82	85.11	121	174.68
5	6.41	44	36.46	83	85.72	122	177.65
6	7.19	45	37.79	84	87.89	123	178.76
7	7.94	46	38.15	85	89.62	124	181.63
8	8.46	47	38.46	86	92.66	125	185.45
9	8.76	48	39.87	87	94.77	126	187.99
10	9.09	49	40.56	88	96.93	127	191.41
11	10.08	50	42.08	89	99.49	128	192.85
12	10.89	51	43.19	90	101.20	129	197.26
13	11.96	52	43.48	91	103.31	130	198.54
14	12.23	53	45.25	92	105.01	131	200.78
15	12.63	54	46.43	93	105.92	132	203.22
16	13.05	55	48.15	94	108.59	133	206.16
17	13.93	56	48.69	95	110.30	134	209.93
18	14.57	57	49.76	96	112.97	135	211.07
19	15.17	58	50.55	97	118.50	136	213.61
20	16.02	59	50.84	98	122.37	137	216.73
21	16.94	60	52.01	99	122.97	138	219.00
22	17.59	61	53.70	100	125.14	139	222.82
23	18.35	62	56.91	101	127.92	140	224.22
24	18.75	63	58.44	102	129.16	141	225.23
25	20.00	64	59.33	103	130.43	142	227.93
26	20.93	65	60.38	104	132.58	143	232.23
27	21.73	66	61.63	105	135.86	144	234.72
28	22.50	67	63.05	106	137.96	145	236.23
29	22.94	68	64.26	107	140.16	146	237.45
30	25.30	69	66.20	108	141.35	147	243.83
31	25.50	70	66.95	109	146.00	148	246.54
32	26.11	71	69.31	110	146.50	149	253.39
33	26.82	72	69.67	111	152.80	150	256.18
34	27.14	73	71.93	112	154.21	151	261.31
35	27.43	74	74.23	113	156.63	152	270.98
36	28.41	75	75.79	114	158.91	153	275.81
37	29.90	76	76.27	115	159.61	154	280.04
38	30.39	77	77.70	116	162.11	155	292.94
39	32.08	78	80.33	117	165.35	156	305.16

The double and the triple state degeneracy (ω_i): [{4.22, 4.65}; {7.19, 7.94}; {8.46, 8.76}; {10.08, 10.89}; {12.23, 12.63}; {13.05, 13.93}; {16.02, 16.94}; {18.35, 18.75}; {20.00, 20.93}; {22.50, 22.94}; {25.30, 25.50}; {26.11, 26.82}; {27.14, 27.43}; {34.07, 34.46, 34.77}; {38.15, 38.46}; {43.19, 43.48}; {48.15, 48.69}; {50.55, 50.84}; {66.20, 66.95}; {69.31, 69.67}; {85.11, 85.72}; {105.01, 105.92}; {122.37, 122.97} and {146.00, 146.50}] in cm^{-1}.

Table 5. The double and the triple state degree of degeneracy of the clusters, Au_{51-54} at $\Delta E = 0$.

Gold Nanoclusters (AuNCs)	Point Groups (PG) Symmetry	Spectral Range (Min- to -Max) ω_i [cm^{-1}]	Double (D) & Triple (T) State Degeneracy $[DT]^{(pairs)}$	Total Number of Pairs	Total Random Number (RN) of Different States of Equal Energy RN = (D*pairs+T*pairs)	Predicted Spectral Range Only for D, T-Degeneracies. A: Far Infrared FIR, IR - C 200 - 10 cm^{-1}B: Mid Infrared MIR, IR - C 3330 - 200 cm^{-1} X: Lesser than both, A and B
Au_{51}	C_1	3.67-299.21	$D^1 T^0$	1	2	A, B, X
Au_{52}	C_1	2.40-304.36	$D^5 T^1$	6	13	A, X
Au_{53}	C_1	1.41-382.46	$D^5 T^3$	8	19	A, B, X
Au_{54}	C_1	1.46-305.16	$D^3 T^1$	4	9	A, X

All the clusters have occurred below and within the range of Far Infrared FIR, IR-C 200-10 cm^{-1}, as well as Mid Infrared MIR, IR - C 3330 - 200 cm^{-1} Certainly, such kind of spectrum could be highly possible to observe in the experimental calculations, upon availability in the near future. In Table A., the third column shows that the spectral ranges that have been influenced with respect to the size of the clusters, the shape of the structures, and the arrangement of the atoms (inner core, and the overall outer surface of the edges), as well as the short and the long-range interactions due to the inter-nuclear attraction and the repulsive energies (Vishwanathan, 2021; Vishwanathan, 2019). In addition to that due to the degree of degeneracy [which is being composed by] that gives a deep interpretation about the elliptical motion but that could be multiple single motions.

We are the first to present, the vibrational frequencies of bigger-sized clusters (Au_{51-54}) and the shell-like structure (of course, they are part of the family of so-called full-shell clusters) at $\Delta E = 0$ by using the numerical finite-differentiation method with the DFTB approach. We have observed the vibrational spectrum, the minimum starting and the maximal end ranges that vary between 1.4 and 382.46 cm^{-1} at $\Delta E = 0$. Moreover, amazingly the occupancy of the multiple double and the triple state degeneracy that is being revealed on the gold atomic clusters, Au_{51-54} (refer to Table A). Interestingly, more number of the double state degeneracy may depend on the nearest neighboring atoms, and their interactions, as well as the zig-zag circumstances of the outermost surface surrounded by them. We are able to see, a maximum, of 8 total pairs have occurred on the Au_{53} cluster, which is a special case than the others.

5. Conclusions

We have observed the vibrational properties of the gold clusters in order to explore the stability and the structures. We have highlighted a mini formula for the occupancy of

the double-state degeneracy. Above all, we have pinpointed the correct location of the spectrum, through Far Infrared FIR, IR-C 200-10 cm^{-1}, and Mid Infrared MIR, IR-C 3330-200 cm^{-1}. In addition to that, our prediction will help the researchers to develop a range of potential applications such as catalysis, biomedicine, imaging, optics, and energy conversion.

Acknowledgements for Funding

Initially, the main part of this work was strongly supported by the German Research Council (DFG) through project Sp 439/23-1. We gratefully acknowledge their very generous support.

References

Andres, R.P, Bein T, Dorogi, M., Feng, S., Henderson, J.I., et al. (1996). Coulomb Staircase at Room Temperature in a Self-Assembled Molecular Nanostructure. *Science*, 272, 1323-1325.

Bravo-Perez, G., Garzon, I. L., Novaro, O. (1999). Ab initio study of small gold clusters. *Journal of Molecular Structure: THEOCHEM*, 493, 225-231.

Bravo-Perez, G., Garzon, I. L., Novaro, O. (1999). Non-additive effects in small gold clusters. *Chemical Physics Letters*, 313, 655-664.

Choi, Y.C., Lee, H.M., Kim, W.Y., Kwon, S.K., Nautiyal, T., Cheng, D.Y., Vishwanathan, K., Kim, K.S. (2007). How Can We Make Stable Linear Monoatomic Chains? Gold-Cesium Binary Subnanowires as an Example of a Charge-Transfer-Driven Approach to Alloying. *Physical Review Letters*, 98, 076101.

Dong, Y., Springborg, M. (2007). Global structure optimization study on Au_{2-20}. *The European Physical Journal D*, 43, 15-18.

Dugan, N., Erkoç, S. (2008). Stability analysis of graphene nanoribbons by molecular dynamics simulations. *Physical Status Solidi B*, 245, 695.

Dvornikov, M. (2003). Formulae of numerical differentiation. arXiv preprint math/0306092.

Garzon, I. L., Posada-Amarillas, A. (1996). Structural and vibrational analysis of amorphous Au_{55} clusters. *Physical Review B*, 54, 11796.

Griffith, W.P. (1967). *The Chemistry of the Rarer Platinum Metals (Os, Ru, Ir, and Rh).* Interscience Publishers.

Hartley, F.R. (1973). *The Chemistry of Platinum and Palladium: With Particular Reference to Complexes of the Elements.* Applied Science Publishers Ltd.

Huang, X. (2016). *Polymer Ligand Stabilized Fluorescent Platinum Nanoclusters: Synthesis, Characterization, and Their Applications*. Osaka University.

Huang, X., Li, Z., Yu, Z., Deng, X., Xin, Y. (2019). Recent Advances in the Synthesis, Properties and Biological Applications of Platinum Nanoclusters. *Journal of Nanomaterials*, 2019, 6248725.

Li, J., Liu, Y., Zhang, J., Liang, X., Duan, H. (2016). Density functional theory study of the adsorption of hydrogen atoms on Cu2X (X=3d) clusters. *Chemical Physics Letters*, 651, 137-143.

Porezag, D., Frauenheim, Th., Kohler, Th., Seifert, G., Kaschner, R. (1995). Construction of tight-binding-like potentials on the basis of density-functional theory: Application to carbon. *Physical Review B*, 51, 12947.

Press, W.H., Teukolsky, S.A., Vetterling, W.T., Flannery, B.P. (2007). *Numerical Recipes in Fortran*. Cambridge University Press.

Sauceda, H.E., Mongin, D., Maioli, P., Crut, A., Vallee, F., et al. (2012). Vibrational properties of metal nanoparticles: Atomistic simulation and comparison with time-resolved investigation. *The Journal Physical Chemistry C*, 116, 25147-25156.

Sauceda, H.E., Garzon, I.L. (2015). Structural determination of metal nanoparticles from their vibrational (phonon) density of states. *The Journal Physical Chemistry C*, 119, 10876

Sauceda, H.E., Salazar, F., Perez L.A, Garzon, I.L. (2013). Size and shape dependence of the vibrational spectrum and low-temperature specific heat of Au nanoparticles. *The Journal Physical Chemistry C*, 117, 25160-25168.

Seifert, G. (2007). Tight-Binding Density Functional Theory: An Approximate Kohn-Sham DFT Scheme. *The Journal of Physical Chemistry A*, 111, 5609-5613.

Seifert, G., Porezag, D., Frauenheim, Th. (1996). Calculations of molecules, clusters, and solids with a simplified LCAO-DFT-LDA scheme. *International Journal of Quantum Chemistry*, 58, 185-189.

Seifert, G., Schmidt, R. (1992). Molecular dynamics and trajectory calculations: The application of an LCAO-LDA scheme for simulations of cluster- cluster collisions. *New Journal of Chemistry*, 16, 1145.

Siegel, R.W. (1994). Nanostructured materials -mind over matter. *Nanostructured Materials*, 4, 121-138.

Vishwanathan, K. (2018). Bonding Forces and Energies on the Potential Energy Surface (PES) of the Optimized Gold Atomic Clusters by a Differentiation Step-Size (ds = ± 0.01 a.u.) via DFTB Method. *Nanoscience & Technology: Open Access*, 5, 1-4.

Vishwanathan, K. (2019). DFTB Calculations of a shapeless Au_{55} (C_1) nanoclusters. *New Materials, Compounds and Applications*, *3*(2), 53-76.

Vishwanathan, K. (2021). Au_{25}: A tip-enhanced, spinning top - core-shell? The brightest molecular super star among the nanoclusters, Au_{21-25}. *Advanced Physical Research*, *3*(1), pp.19-34.

Warnke, I. (2007). Heat Capacities of Metal Clusters. Diploma Thesis (Research Assistant and Diploma Research), *Saarland University*.

Wu, L., Fang, W., Chen, X. (2016). The photoluminescence mechanism of ultra-small gold clusters. *Physical Chemistry Chemical Physics*, 18, 17320-17325.

Zhang, C., Duan, H., Lv, X., Cao, B., Ablat, A. et al. (2019). Static and dynamical isomerization of Cu_{38} cluster. *Scientific Reports*, 9, 7564.